

Detecting genetic variation and base modifications together in the same single molecules of DNA and RNA at base pair resolution using a magnetic tweezer platform

Zhen Wang¹, Jérôme Maluenda¹, Laurène Giraut¹, Thibault Vieille¹, Andréas Lefevre¹, David Salthouse¹, Gaël Radou¹, Rémi Moulinas¹, Sandra Astete-Morales¹, Pol d'Avezac¹, Geoff Smith¹, Charles André¹, Jean-François Allemand^{2,3}, David Bensimon^{2,3,4}, Vincent Croquette^{2,3,5}, Jimmy Ouellet¹, Gordon Hamilton^{1*}

¹ Depixus SAS, 3-5 Impasse Reille, 75014, Paris, France

² Laboratoire de Physique de l'École Normale Supérieure, ENS, Université PSL, CNRS, Sorbonne Université, Université Paris-Diderot, Sorbonne Paris Cité, Paris, France.

³ IBENS, Département de biologie, École normale supérieure, CNRS, INSERM, PSL Research University, 75005 Paris, France.

⁴ Department of Chemistry and Biochemistry, UCLA, 607 Charles E Young Drive East, Los Angeles, 90095, USA.

⁵ ESPCI Paris, PSL University, 10 rue Vauquelin, 75005 Paris, France.

* Corresponding author

Abstract

Accurate decoding of nucleic acid variation is important to understand the complexity and regulation of genome function. Here we introduce a single-molecule platform based on magnetic tweezer (MT) technology that can identify and map the positions of sequence variation and multiple base modifications together in the same single molecules of DNA or RNA at single base resolution. Using synthetic templates, we demonstrate that our method can distinguish the most common epigenetic marks on DNA and RNA with high sensitivity, specificity and precision. We also developed a highly specific CRISPR-Cas enrichment strategy to target genomic regions in native DNA without amplification. We then used this method to enrich native DNA from *E. coli* and characterized the differential levels of adenine and cytosine base modifications together in molecules of up to 5 kb in length. Finally, we enriched the 5'UTR of FMR1 from cells derived from a Fragile X carrier and precisely measured the repeat expansion length and methylation status of each molecule. These results demonstrate that our platform can detect a variety of genetic, epigenetic and base modification changes concomitantly within the same single molecules.

Keywords: DNA, RNA, nucleic acid, magnetic tweezers, MTs, base modification, methylation, epigenetics, DNA base modifications, RNA base modifications, alternative splicing, single molecule, FMR1, repeat expansion, enrichment, DNA fingerprint, RNA fingerprint, oligonucleotides, antibodies.

Detecting genetic variation and base modifications in DNA and RNA

Introduction

Next-generation sequencing (NGS) has enabled a revolution in our understanding of genomics. Current NGS instrument systems are highly scalable and flexible and generate accurate sequence data that is valuable in many different applications¹⁻³. Progress has been rapid due to the dramatic reduction in sequencing costs and continuous improvements to data quality. Despite these advances, determining the entire genetic sequence of a sample with short-read NGS systems has proven too expensive for many routine research and translational experiments. In addition, epigenetic and long-range structural data are also typically missed, with many NGS assays at best only providing indirect measurements of genome function. For transcript analysis, for example, the conversion of RNA to cDNA erases the numerous modifications on RNA bases and creates quantification bias after multiple cycles of amplification⁴.

To meet these challenges, different NGS workflows have been developed, each with its own benefits and trade-offs. Some of the most widely used workflows to reduce sequencing costs rely on capturing specific regions of the genome, using either PCR amplification or affinity purification, and then sequencing these focused libraries using short read technology⁵⁻⁸. Compared to full genome sequencing, these protocols dramatically reduce per-sample costs as multiple samples can be pooled and multiplexed; however, because these methods involve sample amplification, this benefit comes at the penalty of loss of epigenetic information and the introduction of bias into the results⁹. Recently amplification-free Cas9-based enrichment strategies have been attempted by several groups¹⁰⁻¹² but typically only achieve an enrichment of 20- to 60-fold (compared to 10,000-fold for PCR)¹³.

By contrast, the ability to generate long-range genomic information has required the advent of longer read-length, single-molecule sequencing approaches, for example using nanopores (Minion, Oxford Nanopore)¹³ and zero-mode waveguides (Sequel, Pacific Biosciences)^{14,15}. Although these platforms have proven to be useful for closing gaps in short read sequencing, and in providing important long-range structural information, they lack the per-read accuracy of NGS, and to date have only characterized a limited range of epigenetic modifications.

To complement these existing systems, we are developing a universal platform for genomic and epigenomic analysis that records the complexity of information on native nucleic acid molecules of both DNA and RNA. Both our genomic and epigenomic analytical approaches are based on MT technology, which has been used extensively for elucidating the function of DNA polymerases and different accessory proteins required for DNA replication¹⁶⁻²⁰.

In a typical experiment, DNA molecules are converted into hairpin structures. Each hairpin is then attached by one of its free ends to a micron-scale paramagnetic bead and anchored by the other end to a planar glass surface. When a carefully calibrated magnetic force (of greater than approximately 15 pN) is applied to the tethered beads, these hairpins mechanically open (“unzip”) to become single-stranded. They then reform (“re-zip”) again with relaxation of the force (Figure 1A)²¹. When ligands that bind DNA are introduced into the system, their bound presence on the molecule can disrupt hairpin unzipping or re-zipping, and the position of these transient blockages can be mapped to the sequence of the hairpins (Figure 1B). The blocking state is transient, and the average blocking time reflects the off-rate of the bound molecule while the on-rate defines the probability of observing the bound state. As the process is non-destructive, the same hairpin molecules can be opened and closed many times in a single experiment, enabling the detection of either nucleic acid sequence or different base modifications with increasingly high levels of confidence through repeated interrogation. To our knowledge, this feature is unique among single molecule genomic technologies and allows both the mapping of multiple ligands on the same molecule (either simultaneously or sequentially), and the application of error correction techniques to improve analytical accuracy.

Detecting genetic variation and base modifications in DNA and RNA

Here we demonstrate the performance of a new genetic analysis platform that improves the measurement accuracy and experimental operation of MTs to enable the accurate analysis of long molecules of DNA and RNA. Previous versions of MT instruments relied on diffraction from a single light source to measure the Z-position of paramagnetic beads, with single base accuracy reported only for fragments of DNA less than 80 base pairs²². To allow the analysis of longer molecules with greater accuracy, a new instrument was designed (manuscript in preparation) with two important changes. Firstly, a new illumination strategy was developed based on stereo darkfield interferometry (SDI) in which paramagnetic beads are illuminated by a pair of light sources to generate a correlated set of diffraction fringes. Accurate measurement of the relative displacement of these fringes in the X axis corresponds to the position of the bead in the Z axis (Patent EP3181703B1). In addition, improvements to the temperature stability were implemented to allow experiments of longer duration which are required for the analysis of multiple features on these molecules. We used this new instrument to detect the underlying sequence structure and a range of base modifications together in model templates of DNA and RNA. In addition, we developed a novel enrichment method to target genomic regions in native DNA samples without the need for amplification. This allowed us to analyze both methylation restriction systems of *E. coli* together in the same individual DNA molecules, and to characterize both the underlying structural variation and epigenetic modification of single molecules of native DNA molecules from the clinically important gene, *FMRI*. Improvements to the accuracy, usability and throughput of this MT platform will expand the application of these methodologies across many areas of genomic research to reveal the details underlying the complexity of genetic control and regulation.

Results

Characterization of a new generation of MT instrument with single base resolution.

To extend the application of MTs to genomic studies, it was important to test the new SDI instrument system for its positional precision with longer nucleic acid molecules. For these studies we constructed a 600 bp double stranded DNA hairpin with four binding sites for an 11-mer oligonucleotide and tracked the bead positions during 100 cycles of zipping and unzipping under magnetic force. The positions of all four blocking positions were within 1 base pair of the expected locations. We then extended the analysis to a longer 5 kb hairpin and determined that the resolution of the instrument was 1 bp or less for molecular lengths up to 1.5 kb, with precision decreasing as a function of molecular length as expected. We attributed the improved positional accuracy of the SDI instrument to the lower instrument noise (0.9 bp vs 2 bp) (Supplemental Fig. 1). We therefore concluded that the SDI instrument could measure genomic features to a precision of 1 bp for molecules up to 1.5 kb, and that this improvement would permit the more accurate analysis of DNA and RNA for genomic applications.

Identification and mapping of DNA base modifications

Having shown the potential of the new MT instrument to accurately map oligonucleotide blocking positions, we were interested to test if antibodies selected for binding to different DNA base modifications could also block hairpin reformation and whether these blockages could identify and locate the position of the underlying base changes.

We assembled a DNA hairpin from chemically synthesized oligonucleotides that contained seven different base modifications (5-methylcytosine (m⁵C), 5-hydroxymethylcytosine (hm⁵C), 5-carboxylcytosine (ca⁵C), 5-

Detecting genetic variation and base modifications in DNA and RNA

formylcytosine (f⁵C), 3-methylcytosine (m³C), N6-methyladenine (m⁶A), and 8-oxoguanine (8-oxoG)) at defined locations. We then tested commercially available antibodies for their sensitivity and specificity to accurately detect these modified bases (Figure 2a). For 6 out of the 7 modifications, we identified an antibody that could detect the expected modification in more than 95% of the molecules analyzed (Table 1). Furthermore, by correlating these blockages to the positions of a series of reference oligonucleotides, all the antibodies tested mapped the base modification within 1 bp of the expected location on average (Figure 2D).

For four of the antibodies tested (those raised against hm⁵C, ca⁵C, m⁶A and 8-oxoG), the binding was highly specific, and the blockages corresponded to the expected position of the cognate antigen (Figure 2b). For two other antibodies (raised against m⁵C and f⁵C), we detected the expected base, but also identified a second binding position that could be mapped to the position of one of the other base modifications (anti-m⁵C cross-reacted with hm⁵C, and anti-f⁵C cross-reacted with ca⁵C, Figure 2B).

We tested whether we could distinguish true positive blockage events from those occurring through cross-reactivity by comparing the binding times and frequencies (proportion of cycles for which blockage occurred) for both the m⁵C and f⁵C antibodies. For anti-m⁵C, we found that by applying a simple threshold for binding time and frequency we could cluster the true positives from off-target interactions (Figure 2c). This suggested that the interaction of the anti-m⁵C antibody to m⁵C was of a higher affinity than the binding to hm⁵C. By contrast, no such simple cut-off could be applied to the anti-f⁵C antibody (data not shown). However, because we can test different antibodies sequentially on the same DNA molecules, we could cross-correlate blockage data to identify the correct base modification. For f⁵C, for example, comparing the blockages obtained with anti-f⁵C and anti-ca⁵C improved the specificity of f⁵C detection to 100% (Table 1). Lastly, for m³C modification, we were unable to get repeatable data due to batch differences with the anti-m³C polyclonal antisera that we tested (no monoclonal antibodies are currently available for this modified base). In conclusion, commercially available antibodies were able to create blockages on synthetic hairpins and these could be used to detect and precisely locate base modifications tested. However, we note that polyclonal sera may not be reliable reagents for such single molecule analyses.

Characterization of splicing isoforms by oligonucleotide hybridization signature

As our platform can analyze molecules up to 5 kb with high precision, we chose the well-studied mouse myogenic model to test the applicability of MTs to the identification and quantification of full-length splice variants²³. We selected two genes known to be alternatively spliced during mouse myogenesis, one that is expressed in only two isoforms (*CAPZB*), and a second gene (*RBM9*), which has a more complex splicing pattern (Figure 3a). Starting with full-length mRNA, we generated cDNA amplified using a linear amplification method and then incorporated these cDNAs into hairpins (Supp figure 2). Using a panel of oligonucleotides, we could produce specific binding signatures that were dependent on the isoform (Figure 3b). For *CAPZB*, we found that only 5% of the molecules present in myoblast cDNA included exon 8 whereas the number of molecules containing this exon increased to 65% in myotubes. These results were supported by splicing PCR analysis on independent samples from both cell types (Suppl. Figure 3) and agree with the findings of Bland et al²⁴. For *RBM9*, four exons have been shown to be alternatively spliced giving rise to nine possible isoforms. We observed the expression of six of the nine possible isoforms, and four of these (isoforms 1, 2, 5 and 6) were significantly enriched in only one cell type reflecting a change in their distribution upon muscle differentiation (Figure 3a). To validate the measurement accuracy of our approach, we compared the expression levels of the different genes obtained by measurement of oligonucleotide hybridization in our instrument with read count data generated by the PacBio platform. For both *CAPZB* and *RBM9*, there was a close correlation in the measurement of the different isoform expressions (Figure 3a).

Detecting genetic variation and base modifications in DNA and RNA

Decoding RNA with short oligonucleotide probes

We next investigated whether we could decode an RNA template using a set of overlapping oligonucleotide probes and tested if short 3-mers could generate blockages of sufficient binding strength and duration to allow accurate positional information. We observed that modifications to the oligonucleotide backbone structure and the incorporation of intercalators significantly improved binding stability.

A 100-base synthetic RNA template was ligated into a hairpin otherwise composed of DNA and probed for blockage events with a set of 3-base modified oligonucleotides. Based on these blockage positions, we were able to reconstruct the sequence of the 100 bases of RNA. Because the probe binding positions overlap, each base was detected by three different oligonucleotides which allowed for redundancy in the sequence determination and permitted a simple error correction algorithm to generate the most energetically favorable sequence. We were able to reconstruct sequence information from 20 of these molecules, obtaining sequence accuracies of between 70% and 96% for the individual 100-base RNA molecules, and a consensus sequence accuracy of 95% (Fig 3c).

Detecting epigenetic modifications in RNA

Having shown that antibodies could be used to reveal the identity and position of base modifications in DNA, and that the platform could also be used to decode RNA directly using oligonucleotide probes, we were interested in analyzing the potential of antibodies to locate the position of different RNA base modifications. We constructed a hybrid DNA-RNA hairpin comprising 95-bases of synthetic RNA containing both m⁵C, m⁶A and inosine RNA base modifications ligated within a DNA backbone (Figure 4A). The positions and durations of transient blockages for a range of commercially available antibodies were then determined.

The m⁵C modification in RNA was detected with high sensitivity (we detected the modification on 99.1% of the molecules, n=111, Figure 4D). However, this antibody also generated blockages at base positions corresponding to the m⁶A base modification for 29 beads analyzed (n=111 molecules). To improve specificity of base modification detection by filtering these false positive peaks, we compared the binding profiles for different antibodies. In the case of anti-m⁵C antibody, we could eliminate blockages to m⁶A by subtracting of the positions observed with anti-m⁶A antibodies to increase the specificity to 98% (Figure 4B and D).

For m⁶A, by contrast, all three antibodies tested showed lower sensitivities (76%-93%, Figure 4D) than was seen for m⁵C detection. However, when combining the blockage data from all three m⁶A antibodies, we saw a modest reduction in sensitivity (to 89.3%; Figure 4b and 4d) but more importantly, raised the specificity of detection to 96%. This high level of confidence in base modification calling as well as high specificity is essential for detecting base modification on native RNA. Finally, we were unable to find a suitable antibody to inosine due to a high level of cross reactivity against all bases in the test template (data not shown).

Next, we determined the precision of mapping RNA base modifications by using a set of reference oligonucleotides targeted to the DNA handles of the hairpin to provide a series of calibration measurements. We observed a systemic difference (of 5 bp) in the position of the antibody blockage compared to the actual position of the RNA base modification based on the primary sequence, and this effect was observed for all antibodies tested. To investigate the cause of this bias, we hybridized a set of oligonucleotide probes to the region of RNA containing each base modification. These probes also showed bias in their calculated binding location, suggesting that this was due to the differential stretching of RNA compared to DNA²⁵⁻²⁷. Comparing the binding positions between these internal

Detecting genetic variation and base modifications in DNA and RNA

probes and antibody blockages allowed correction of this stretching effect and the accurate localization of the underlying base modification to within two bases (Figure 4c).

Targeting genomic loci in native DNA using a CRISPR-Cas enrichment protocol.

To enable the analysis of epigenetic modifications at defined loci within native DNA, we developed an amplification-free protocol for sequence-based enrichment. We chose the CRISPR-Cas meganuclease system as a starting point because this method has the potential to be highly selective and is compatible with parallelization and a low amount of starting material. We observed that both Cas9 and Cas12a proteins remain bound to their targeted DNA fragments even after cleavage, and thus effectively shield the cut site from exonuclease digestion (Supp Figure 4). To exploit this finding, we developed a two-step method to target the region of interest where in the first step, the region of interest was flanked by a pair of CRISPR-targeted Cas12a proteins (Figure 5a). Enrichment of the targeted region was accomplished by digesting the non-targeted region using exonucleases. In the second step, a 3' overhang was created by targeting CRISPR-targeted Cas9d between 100 to 200 bases from the Cas12a site and, using lambda exonuclease, digesting from the end of the fragment up until the Cas9d. These ssDNA overhangs were then used to assemble a hairpin by the ligation of Y-shape and loop sequences.

We quantified our approach and validated that it could retain epigenetic modifications by isolating four different sized DNA fragments from *E. coli* genomic DNA, ranging from 0.8 to 5 kb. Quantification by qPCR showed that we recovered between 55% and 75% of the starting material for the four fragments after the first step, and between 35% and 55% after the second step whereas the non-protected DNA decreased to less than 0,05% of the starting material (Figure 5b). Most of the loss of material can be accounted for by the two purification steps required during the protocol (almost 40% lost after the Cas9d step, Figure 5b control without exonucleases). All four fragments were successfully converted to hairpin molecules that could be analyzed on our platform (Figure 5c).

We chose to study *E. coli* DNA because of the activity of the well-characterized *dam* and *dcm* methylases that modify A and C residues at well-defined sequence motifs, and this allowed us to validate detection of both m⁶A and m⁵C in native DNA via our antibody-based MT approach. First, we identified individual molecules using a single four-base oligonucleotide (CAAG) that bound multiple times to produce a characteristic 'genomic fingerprint' to determine the identity of the hairpin. All the functional hairpins could be assigned to one of the four targets (n=359 molecules), demonstrating that the enrichment strategy was 100% specific (Figure 5c). Next, we added the anti-m⁶A and anti-m⁵C antibodies sequentially to create blockages in the closing of the hairpin structures and then matched these to the expected locations of the *dam* and *dcm* recognition sequences (GATC and CCwGG respectively). All expected positions were modified, albeit at different levels, which, in most cases, was over 50% and approached 100% (Figure 5d). However, there were some instances where we detected only a low level of methylation (m⁵C at position 1186, and m⁶A at positions 953 and 1358). We also monitored the level of m⁵C methylation for all the isolated fragments (Figure 5e) and we observed systematic variation in levels of methylation dependent on the genomic position, consistent with data previously reported for exponentially growing cells²⁸. We concluded that the Cas-based enrichment method very effectively targets specific loci to allow detection of epigenetic base modifications in our platform.

Enrichment of specific regions from human genomic DNA

To demonstrate that our PCR-free enrichment protocol can also enrich human genomic fragments, we isolated four regions implicated in human diseases. We chose *FMR1* and *C9orf72* for their short tandem repeat regions, which

Detecting genetic variation and base modifications in DNA and RNA

are difficult to measure on other platforms, and *SEPT9.1* and *SEPT9.2* which both have CpG islands where their methylation status has been implicated in colorectal cancer^{29–31}. We performed the enrichment from cultured HEK cells and were able to identify all four regions in our platform. The identity of these fragments was confirmed using the specific blocking pattern produced by the oligonucleotide CAAG (Suppl Figure 5) and as with our enrichment from *E. coli*, we did not observe any hairpins containing off-target DNA. Therefore, our enrichment worked on human gDNA as well as on *E. coli* and showed 100% target specificity.

Analysis of short tandem repeat length and methylation status at the FMR1 locus

To demonstrate the ability of our platform to extract both genetic and epigenetic information on the same individual molecules, we chose to further focus on Fragile X Syndrome (FXS), a genetic disorder characterized by an expansion in the number of CGG repeats in the 5' untranslated region (5'UTR) of the Fragile X mental retardation 1 (FMR1) gene on the X chromosome³². In addition to the repeat expansion, the FMR1 promoter is also differentially methylated in different disease states³³. We were interested to test if our workflow could provide an accurate method to measure the lengths of the trinucleotide repeats and, by preserving epigenetic marks during sample preparation, allow the analysis of both features together in the same single DNA molecules.

In a pilot experiment with genomic DNA isolated from the human HEK cell line, we found that the highly GC-rich CCG repeat sequence created additional spontaneous blockage events, most likely due to the formation of G-quadruplex and other DNA secondary structures. To overcome this effect, we designed new reference oligonucleotides that could form a three-way junction, thereby transiently preventing the hairpin from opening under high force (Supplemental figure 6). Using this strategy, we were able to measure the distance between blockings in the hairpin opening phase rather than in the rezipping phase. This approach was demonstrated by quantifying a normal range of trinucleotide repeats in HEK cells (between 31 and 35, n=26) (Figure 6a and 6c).

We then used our CRISPR-Cas-based enrichment protocol to target the FMR1 locus from cultured cells of sample NA06896, derived from an unaffected female heterozygous carrier of FXS, and measured repeat lengths using the new opening assay for FMR1. We observed that approximately half of the individual DNA molecules had a repeat structure characteristic of a normal allele (between 21–28 repeats, n=30) and the others carried an expanded repeat count (>50 repeats, n= 22, Figure 6a and 6c). These data matched the expected ratio for a heterozygous sample. As expected from these repeats, we observed a greater variability among the molecules with an expanded repeat number compared to the normal allele. 20% of molecules had a repeat number greater than 200, the threshold for the full mutation form of FXS. The other molecules with expanded repeats fell in the range defined for pre-mutation carriers.

Next, we analyzed the methylation status on the same single molecules from NA06896 with an antibody to 5-methylcytosine. For all molecules with over 200 repeats, we observed either no or very low levels of methylation in the promoter region (n=3, Figure 6B). This result was striking in comparison to most molecules in the normal or pre-mutation category which had high levels of methylation at both CpG and non-CpG sites. However, even among these two groups, we did find instances of low methylation, but they were significantly less frequent than the highly methylated loci (figure 6b). Our results were in concordance with Chen et al. (2011) who used a methylation-specific PCR test and reported a lack of methylation on repeats greater than 150, but high levels of methylation for pre-mutation alleles and low levels for normal repeats³⁴. We concluded that our amplification-free enrichment method was effective for targeting FMR1 and for preserving the underlying genetic and epigenetic structure of the locus.

Detecting genetic variation and base modifications in DNA and RNA

Furthermore, the use of a MT instrument was effective in the combined analysis of repeat length and methylation status on individual molecules of DNA.

Discussion

Over the last few years, it has become increasingly apparent that there are areas of genome biology that are difficult to access with NGS technology, such as the accurate detection of base modifications in DNA and RNA, the co-detection of multiple genomic features on the same molecules, and the ability to obtain long-range genomic information³⁵. These questions have fundamental importance to our understanding of how genomes are organized and controlled, and our ability to characterize the different processes leading to disease³⁶. There has therefore been an increasing effort to improve genomics tools that rely on the direct detection of nucleic acid bases and, in particular, single-molecule approaches to identify multiple base modifications.

Here, we present a significant improvement to the accuracy of the well-known MT technology outlined in Ding et al (2012). We demonstrate the application of this new system to the direct detection of both sequence signatures and modified bases together in DNA and RNA molecules and the localization of these features in these templates at base pair resolution. To capture this diversity in native DNA, we developed a highly specific amplification-free workflow for enriching genomic regions in bacterial and human genomes. Because of the non-destructive nature of the MT technology (we typically used 100 open-close cycles in these experiments, but we have extended this to 10,000, unpublished), a wide variety of probes can be tested sequentially to improve the specificity and sensitivity of sequence and base modification detection at the single molecule rather than the consensus level.

The approach we outline here has allowed the unambiguous identification of six modified bases in the same DNA template. To our knowledge, this is the largest number of different base changes that have been detected in an individual template with high accuracy using any genomics approach. NGS-based methods cannot detect these base changes directly and instead rely on the chemical conversion of one base to another^{37,38}. Due to the subtractive nature of the analysis, these approaches generate maps one modified base at a time at the population level. By contrast, single molecule approaches offer the promise of a direct readout of unamplified native DNA changes, and there has been steady progress in the detection of base modifications using nanopores (Oxford Nanopore, ONT) and Single Molecule Real Time sequencing (SMRT, Pacific Biosciences)³⁹⁻⁴¹. These methods detect the modulation in current blockage or polymerase stutter caused by the passage of the modified base. The size of the signal, and the quality of training models and signal processing algorithms dictate the accuracy with which these techniques can distinguish the different modified bases from one another, or from natural bases^{42,43}. Detecting modified bases with SMRT sequencing requires a minimum sequencing fold coverage of between 25x (e.g. for m⁶A) and 250x (e.g. for m⁵C)⁴⁴ while with ONT protocols, the single pass of any individual template through a pore provides only one opportunity to detect modified bases in that molecule.

Using our MT approach, highly accurate detection of multiple base modifications can be achieved by repeated probing of the same templates with different antibody probes and analysis of their binding kinetics. These features overcome both the lack of specificity that has been well documented for ChIPseq-type experiments that use only a single antibody⁴⁵, and the inherent stochastic sampling that contributes to the high error rates often observed in other single molecule approaches. We have tested a number of different antibodies and shown that they have widely varying cross-reactivities. We report high-quality identification of base modifications with monoclonal antibodies,

Detecting genetic variation and base modifications in DNA and RNA

while a poor performance with polyclonal antibodies such as m³C polyclonal sera, a common issue in using these reagents. We anticipate that the standardization of these antibody-based tools and the generation of new appropriately tuned ligands based on proteins that naturally bind to modified bases will greatly assist in the characterization of the landscape of epigenetic changes and damaged bases in DNA. Notice that our method allows quantifying the quality of antibodies at the single molecule level.

Over the 150 base modifications are found in RNA, and whose functions are only just being discovered. It remains a significant technical challenge to identify the many similar chemical moieties at base-pair resolution^{35,46}. As with DNA, single molecule techniques offer significant benefits over current NGS-type approaches in reading the RNA modifications directly in the native strands, rather than indirectly through immunoprecipitation or reverse transcriptase stuttering⁴⁷. We confirmed that the analytical approaches developed for DNA could also be applied to RNA, also a robust template molecule in our system. Individual RNA molecules were identified through tiling of overlapping short probes to determine sequence signatures and antibodies were used to identify and localize two biologically important base modifications present on the same RNA molecules with high sensitivity and specificity. We intend to expand this approach to wider range of RNA base modifications, helping to unlock this important emerging area of biological science.

FMR1 is an example of a clinically relevant gene that is difficult to analyze with short-read technology because the number of trinucleotide repeats required for diagnosis exceeds typical NGS read-lengths, and stitching overlapping reads together creates ambiguity in repeat counting. Furthermore, the repeat itself is composed entirely of GC bases, which prevents accurate amplification during sample preparation. We were interested in studying FMR1 at a single-molecule level because of the link between the epigenetic status of the FMR1 promoter and the number of CCG repeats, and since repeat number and methylation mosaicism are common phenomena in FXS. Analysis of these genetic and epigenetic features on native molecules of FMR1 has been attempted using both SMRT sequencing and nanopore sequencing but in neither case was it possible to perform accurate repeat sizing and methylation analysis on the same single molecules^{48,49}. Our MT platform is well suited to this dual analysis in the same single molecules of DNA. To analyze specific gene loci without DNA amplification, we developed the CRISPR/Cas9 enrichment method that achieved target specificities that are far greater than we have seen reported elsewhere in the published literature¹⁰⁻¹². From human genomic DNA, we enriched fragments containing FMR1 and observed that the allele frequency of expanded repeats to normal was in the expected 1:1 ratio for a heterozygous sample. We were able to accurately measure the length of the trinucleotide repeat in normal alleles and those in the full-mutation state, as well as identify DNA molecules in a pre-mutation status. In addition, the same single molecules were interrogated for promoter methylation, and we identified that all molecules that had >200 repeats were almost entirely unmethylated. These data were in broad agreement with Chen et al (2011) using orthogonal methods on the same sample³⁴. Our results suggest that the combination of our highly specific targeted enrichment together with the MT assay has the potential for a fast and accurate workflow for the detection of multilayered patterns of information, allowing comprehensive epigenetic profiling in clinical samples from a single assay.

In conclusion, we have shown how a MT platform can be used to perform a variety of genomic and epigenetic analyses on kilobase length single molecules of both DNA and RNA and how these analyses can be performed sequentially to reveal multiple features from the same molecules. Furthermore, as MTs are already commonly used for characterizing protein/nucleic acid interactions, we see the utility of this technology to develop a powerful multiomic analysis platform with which information on sequence variation and epigenetic modification is combined with that from the binding and modification of protein complexes that regulate gene expression. To this end, we are

Detecting genetic variation and base modifications in DNA and RNA

also planning to integrate fluorescence detection into the MT technology, offering a broad platform for the analysis of proteins and nucleic acid interactions⁵⁰.

Efforts are also underway to scale the technology from current throughputs, where hundreds of molecules are analyzable in parallel, up to millions of molecules. This will be achieved using both optical and all electronic methods (patent EP3090803B1) and will allow the technology to be used either for genome- and transcriptome-wide analyses or, alternatively, when in combination with our amplification-free enrichment method, for fast and cost-effective panel-based testing for disease-causing genes at high depths of coverage. In addition, we are working to further reduce the required starting material for library construction to levels that will open up the areas of single-cell genomic, epigenomic, and (epi)transcriptomic analysis.

Materials and methods

Hairpin construction and characterization of the new magnetic tweezer instrument

For measuring the precision of the new instrument, the DNA epigenetic hairpin (600 bp) described in the next section was prepared and attached to paramagnetic *MyOne* T1 streptavidin beads (DynaL/Life Tech).

To measure Brownian noise on the new SDI instrument, a hairpin was constructed by amplifying a 5 kb fragment from the PhiX174 genome. Each primer used (see Supplementary table 1) contained a non-palindromic restriction site (BsaI), which introduced two distinct 4-base overhangs at each end of the PCR fragment after digestion. These 4-base overhangs allowed the directional cloning of the Y-shaped adaptor required for bead and surface attachment (Triple-biotin/PS866) as well as the synthetic loop (PS359) at the other extremity (Supplemental table 1). The resulting hairpins were bound to *MyOne* T1 streptavidin beads (DynaL/Life tech) and injected into a flow cell for capture through a splint oligonucleotide (PS867) on the surface. This was achieved by first covalently attaching an oligonucleotide (PS625) containing a DBCO group at the 3' end to an azide coated coverslip using copper-free click chemistry that would form the base of the flow cell. Ten-base reference oligonucleotide in ABB6 buffer (20 mM Tris HCl pH 7.5, 150mM NaCl, 2 mg/mL BSA, 0.1% sodium azide) was injected into the flow cell and test cycles (of increasing and decreasing magnetic force) were performed at 18 °C. The noise variation between successive camera frames (frequency 1/30 sec.) was extracted and plotted for all the oligonucleotide binding positions on each hairpin.

Hairpin construction for DNA epigenetic detection

Seven synthetic oligonucleotides, each containing a DNA base modification, were obtained from Eurogentec along with the complementary oligonucleotide that allows construction of the synthetic linker (Supplemental table 1). A synthetic 175 bp PCR fragment was digested with BsaI to generate a non-palindromic 4-base overhang and ligated to the synthetic linker. A second PCR fragment of 250 bp, also digested with BsaI to generate a different compatible 4-base overhang, was ligated at the second extremity of the synthetic fragment. The resulting fragment was digested with BsmBI to generate third and fourth non-palindromic sites at either end of the 550 bp fragment to allow the ligation of the Y-shape (triple-biotin/PS866) and the synthetic loop (PS359). The resulting hairpin was purified on an agarose gel and attached to paramagnetic *MyOne* T1 streptavidin beads (DynaL/Life Tech).

Detecting genetic variation and base modifications in DNA and RNA

Detection of base modifications in DNA

For base modification detection, commercial antibodies raised against the DNA base modifications present on the test hairpin were used. For m⁵C, we used the ICC/IF clone from Diagenode (C15200003) at a dilution of 1:500. For m⁶A, we used the Cell Signaling Technology clone D9D9W at a dilution of 1:300. For 8-oxoG detection, we used the clone 15A3 from R&D Systems Europe Limited (4354-MC-050) at a dilution of 1:500. For hm⁵C, we used the clone RM236 from Invitrogen™ (15815913) at a dilution of 1:500. For ca⁵C detection, we used the clone RM24 1-A3 from AbCam at a dilution of 1:500. For f⁵C, we used the polyclonal antibody mix from Active Motif (61228) at a dilution of 1:500. These antibodies were diluted in ABB6 buffer and supplemented with 500nM of the reference oligonucleotide OR3 for precise mapping of the modification of the hairpin. At least 100 cycles of opening-closing were performed for each antibody and the binding of the oligonucleotide as well as the antibodies were aligned to the known sequence of the hairpin.

Hairpin construction for RNA epigenetic detection

A synthetic hairpin was constructed from synthetic RNA fragment flanked by 600 bp and 400 bp DNA fragments. In brief, the three RNA oligonucleotides (Eurogentec) containing three different base modifications: m⁶A, inosine and m⁵C, separated by 20 nucleotides, were assembled by hybridization and ligation over a complementary DNA strand using T4 RNA ligase 2 (NEB). To construct the hairpins, the resulting synthetic RNA/DNA hybrid fragment was ligated to both the 600 and 400 bp DNA fragments before ligating a loop (PS359) and Y-shape (triple-biotin/PS866) at either end using T3 DNA ligase (NEB). The hairpins were gel purified and attached to paramagnetic MyOne T1 streptavidin beads (DynaLife Tech).

Epigenetic detection of RNA using antibodies

To detect epigenetic base modifications on the synthetic RNA-containing hairpins, several commercially available antibodies were used. For m⁵C, the ICC/IF (C15200003) mouse monoclonal antibody from Diagenode was used at 1:250. For m⁶A, we used the rabbit monoclonal m⁶A antibodies were from Cell Signaling Technology (clone D9D9W, at 1:500 dilution), the RevMAb Biosciences (clone RM362, at 1:300 dilution) and the mouse monoclonal recombinant AbFlex m⁶A antibody (rAb) from Active Motif (at 1:300 dilution). A mixture of reference DNA oligonucleotides that correspond to the position of the modified nucleotides was used to compare with antibody binding (the last base at the 5' end of the oligonucleotide hybridizes with the modified base, blocking the fork in the same position as the antibody). Each experiment was recorded for more than 100 cycles. For all the experiments, the antibody was used together with reference oligonucleotides in oligonucleotide binding buffer (PBS pH 7.4, 2 mg/ml BSA, 0.1% sodium azide).

mRNA isolation and cDNA library preparation

C2C12 myoblast and myotube cells were gifts from Dr. Herve Le Hir's laboratory, from the biology department at ENS, Paris, France. Total RNA was extracted with Trizol (ThermoFisher) following the manufacturer's instructions and treated with TurboDNase (Ambion).

The full-length cDNA was synthesized from 2 µg of total RNA using the TeloPrime Full-Length cDNA Amplification Kit (Lexogen) and the final full-length cDNA library was amplified 15-20 cycles according to the manufacturer's instructions.

Detecting genetic variation and base modifications in DNA and RNA

Alternative splicing PCR

We performed classical PCR for splicing isoform detection for CAPZB and RBM9 using primers to the flanking constitutive exons. PCR was performed using DreamTaq (Fermentas) for 30 cycles of denaturation at 95°C for 60 sec., followed by a step at 60°C for 30 sec. and elongation at 72 °C for 4 min. The resulting PCR sample was loaded onto a fragment analyzer (Agilent Technology) and the ratios between different peaks were calculated using the area under the curves. A list of the primers used is given in Supplementary Table 1.

Loop PCR and hairpin preparation

Loop PCR was performed using a forward primer containing either an isoG base (to stop the polymerase and therefore create a 5' overhang of known sequence) or a nickase site, and a reverse primer containing a loop sequence (the sequence of the oligonucleotides used can be found in Supplemental Table 1). PCR was performed with Phusion DNA polymerase (NEB) and we used a slow ramp for the elongation step from 72°C to 98°C to allow the synthesis of the loop on the reverse primer. After 20 to 40 cycles of PCR, depending on the expression of the target, exonuclease I (ExoI) was added (NEB) to remove the single-stranded DNA bearing a 5' loop as well as the remaining primers. Two more cycles were performed to fill in DNA molecules with a 3' loop, and a second ExoI step was used before the PCR products were purified with columns (Qiagen or NEB) or Kapa beads (Roche Diagnostics). When isoG forward primer was used, a Y-shape containing an isoC overhang was ligated using T4 DNA ligase (Enzymatics), followed by agarose gel purification. In the case of the nickase site, PCR fragments were treated with Nb.BbvCI nickase (NEB) before purification and ligating the Y-shape with the correct overhang. The final hairpins were attached to MyOne T1 streptavidin beads (Dyna/Life Tech).

Quantification of splicing isoform hairpins by magnetic tweezer analysis

For the analysis of splicing isoforms, a set of oligonucleotides were designed for the two genes studied that hybridized to both constitutive exons and alternatively spliced exons (Supplemental table 1). The concentration of each oligonucleotide was optimized such that their binding rates (proportion of cycles for which blockage occurred) were similar. The alternative splicing isoforms were determined by the presence or absence of the oligonucleotides binding to the alternative exons. We performed three technical replicates (hairpin construction from the same full-length cDNA library) for three biological replicates (RNA from different cell passages). For each gene, more than 100 beads were recorded, and the identities of the isoforms were determined from hybridization patterns. The proportion of each isoform was calculated for all beads analyzed per technical replicate and represented as the average of all three biological replicates.

PacBio sequencing

For SMRT sequencing, we used the same reverse loop primer and a forward primer integrating a four-base barcode that allows multiplexing of different samples. PCR was performed using Phusion DNA polymerase, with HF buffer for CAPZB, and GC buffer for RBM9. The resulting PCR fragments were purified on agarose gel and multiplexed before SMRT sequencing (Eurofins Genomic).

To improve the assignment rate, we took the unassigned reads and re-mapped them specifically to the two genes with all the isoforms using Burrow Wheeler Aligner (BWA). The resulting BAM files were converted to SAM files and custom scripts were used to re-assign the mapped sequences to correct samples according to the barcodes. The

Detecting genetic variation and base modifications in DNA and RNA

CIGAR tag in SAM files for each sequence was used, and any reads not mapping from the beginning of the sequences were discarded. In addition, any reads that did not map to either strand were also discarded. The resulting sequences were searched for barcode at the beginning or end of the reads depending on the mapping orientation, and any chimeric reads were cut and searched for barcodes. If both parts of the chimeric sequences could be correctly assigned, the reads were split into the correct demultiplexed sample files. If the barcode was too short, the reads were discarded, and if the barcode was wrong for the mapped sequence, these reads were discarded but counted towards the 'mismatch' number. In the end, all the correct sequences were pooled for each sample and output as a BED file.

Magnetic tweezer analysis of RNA using short oligonucleotide probes

For decoding of RNA using short oligonucleotides, a synthetic fragment of 100 nucleotide 2'-*O*-Me RNA and its complementary DNA was ligated to 170 bp and 250 bp DNA fragments at either side using T3 DNA ligase. The resulting sequences were ligated to a loop (PS359) and Y-shape adaptor (triple-biotin/PS866) using T3 DNA ligase. The hairpins were agarose gel purified and attached to MyOne T1 streptavidin beads (DynaLife Tech). The attached hairpins were then ligated to the oligonucleotide at the surface of the flow cell using T3 DNA ligase (Enzymatics). After the ligation step, unligated molecules were washed using 20mM NaOH followed by neutralization with 50mM Tris-HCl. The methylation group of 2'-*O*-Me RNA bases protects the ribose from hydrolysis, allowing the washing step with NaOH.

After defining the optimal force to open and close the hairpins, we injected the oligonucleotides into the flow cell sequentially and recorded at least a hundred cycles. Each 3-base oligonucleotide was tested individually at a concentration varying between 0.5 and 5 nM along with reference oligonucleotides (at 150 nM). Blocking positions and time of blockages were extracted for each cycle for each bead and analyzed using our custom developed software.

Enrichment using Cas proteins

E. coli genomic DNA was extracted using Quick DNA Plus kit from liquid culture of NEB® 5-alpha Competent *E. coli* (NEB #C2988) grown in LB medium according to the protocol provided by the manufacturer (Zymo Research). Purified NA06896 DNA was obtained from the Coriell Institute.

CRISPR-Cas12a (Alt-R® CRISPR-Cpf1) and CRISPR-dCas9 (Alt-R® S.p. dCas9) were purchased from IDT. All crRNA and tracrRNA guide RNA, either for Cas12a or Cas9, were chemically synthesized by IDT. For each target, two Cas9-crRNA were designed to flank the region of interest to be protected and two Cas12a-crRNA at least 100 bases away from the Cas9-crRNA position. (A complete list of crRNA is available in Supplemental Tables 2 & 3).

For the Cas9 gRNA, each crRNA–tracrRNA duplex was prepared independently by mixing 1 pmole of tracrRNA with 2 pmoles of crRNA in Nuclease Free Duplex Buffer (IDT), heated at 95°C for 5 min., then cooled at in successive steps at 80 °C for 10 min., 50 °C for 10 min., and then 37 °C for 10 min. Each Cas9 protein was loaded with a gRNA complex separately in NEB3.1 Buffer (100 mM NaCl, 50 mM Tris-HCl, 10 mM MgCl₂, 100 µg/ml BSA, pH 7.9) at 25 °C for 15 min. at room temperature at a final concentration of 500 nM for dCas9 and 1 µM for the RNA guide.

Detecting genetic variation and base modifications in DNA and RNA

crRNA guides for Cas12a were folded in NEB2.1 buffer (50 mM NaCl, 10 mM Tris-HCl, 10 mM MgCl₂, 100 µg/ml BSA) at 80 °C for 10 min., followed by a step at 50 °C for 10 min., then 37 °C for 10 min. Each Cas12a/crRNA complex was assembled in NEB2.1 buffer supplemented with 10 mM DTT for 15 min. at room temperature at a final concentration of 500 nM of Cas12a and 1 µM crRNA.

Enrichment of E. coli targets:

2.6 pmol of each Cas12a/crRNA complex (2 complexes per targets) was mixed with 5 µg of genomic DNA in NEB2.1 Buffer supplemented with 10 mM DTT for 90 min. at 37 °C. A mixture of exonucleases (lambda exonuclease (40 U/µg of gDNA), ExoI, 40 U/µg of gDNA) was added to the reaction and incubated for an additional 90 min. at 37 °C. Inactivation of the reaction was performed using 40 ng Proteinase K and EDTA at a final concentration of 20nM, followed by a purification using 0.8 x KAPA Pure beads (Roche). The DNA was repaired using T4 DNA polymerase (NEB) with dNTP (200 µM) in NEB3.1 buffer to repair the 5' overhang for 15 min. at 12 °C followed by a purification step using 0.8 x KAPA Pure beads. The resulting DNA was incubated with 333 fmol of dCas9/gRNA complex in CutSmart Buffer supplemented with 0.1% Triton X-100 for 60 min. at 37 °C. Lambda exonuclease (20 U/µg of gDNA) was added to the reaction and incubated for an extra 90 min. at 37 °C. The reaction was inactivated using 40 ng Proteinase K and EDTA at a final concentration of 20 nM, followed by purification using KAPA Pure beads (1 x). The enriched fragments, which contained a long 3' ssDNA overhang, were incubated with 1 pmol of target specific biotin, surface and loop oligonucleotide (sequence available in Suppl table 1), 40 U Tag DNA Ligase (Enzymatics), 0.25 U of Bst DNA Polymerase Full Length (NEB) in ThermoPol® Reaction Buffer (NEB) supplemented with 200µM dNTP, 1mM NAD⁺ at 50 °C for 30 min. Excess oligonucleotide was then digested with 25 U ExoI for 30 min. at 37 °C, followed by a purification using KAPA Pure beads (1 x). The DNA fragments were digested with BsaI to generate specific overhangs that allow the ligation of surface specific oligonucleotides (PS1420 and PS867) and the second overhang created at the opposite end was used to ligate the loop (PS421). The resulting hairpin molecules were bound on 5 µg of Dynabeads™ MyOne™ T1 Streptavidin (Dyna/Life Tech) in passivation buffer (PB: PBS pH 7.4, 1mM EDTA, 2 mg/mL BSA, 2 mg/mL pluronic surfactant, 0.6 mg/mL sodium azide) for 60 min. at room temperature. Beads were washed and resuspended in 1x PB prior to loading into the flow cell.

Quantitative PCR of enriched fragments from E. Coli:

The efficiency of *E. coli* target enrichment was quantified by qPCR after both protection steps. For each target, we designed primer pairs between the two dCas9 and a pair of oligonucleotides outside the targets as a negative control. qPCR reactions were performed on a QuantStudio instrument (Applied Biosystems) with the Fast SYBR™ Green Master Mix Kit (Applied Biosystems).

The enrichment efficiency was calculated based on three biological replicates and each qPCR reaction was performed in triplicate. Amplification reactions were performed in final volumes of 20 µL consisting of 1× Fast SYBR™ Green Master Mix, 50 nM of each forward and reverse primer and 8 µL of DNA template (1:700 dilution of the enrichment reaction). The qPCR cycling conditions were as follows: initial denaturation at 95 °C for 10 min., followed by 40 cycles of denaturation at 95 °C for 15 sec., annealing and elongation at 60 °C for 1 min. Melting curves were produced by increasing the reaction temperature from 60 °C to 95 °C. Standard curves were performed using known amounts of *E. coli* genomic DNA. The initial amount of genomic DNA was set as 100% and the efficiency of each protection step was calculated by dividing the quantity of remaining DNA after exonuclease protection by the initial amount of genomic DNA. Two controls were included: 1) the same protocol for all the four

Detecting genetic variation and base modifications in DNA and RNA

targets was performed but without the exonucleases, allowing estimation of the percentage of material lost during the purification; 2) a region outside the four targets was quantified to determine the amount of remaining material not protected after exonuclease digestion.

Enrichment of FMR1 on human genomic DNA:

300 fmol of Cas12a/crRNA complex per μg of gDNA were incubated in NEB2.1 buffer supplemented with 10 mM DTT for 60 min. at 37 °C. A mixture of exonucleases (lambda exonuclease, 20 U/ μg of gDNA) and ExoI, 20 U/ μg of gDNA) was added and the reaction was incubated for another 60 min. at 37 °C. Inactivation of the reaction was performed using 40 ng Proteinase K and EDTA at a final concentration of 20 nM, followed by a purification using KAPA Pure beads (1 x). The 5' overhang was repaired using T4 DNA polymerase (NEB) with dNTP (200 μM) in NEB3.1 buffer for 15 min. at 12 °C followed by a purification step using 0.8 x KAPA Pure beads. The resulting DNA was incubated with 150 fmol of dCas9/gRNA complex per μg of initial gDNA in NEB3.1 buffer for 60 min. at 37 °C. Lambda exonuclease (15 U/ μg of gDNA) was added and the reaction incubated for another 60 min. at 37 °C. Inactivation of the reaction was performed using 40 ng proteinase K and EDTA at a final concentration of 20 nM, followed by a purification using KAPA Pure beads (0.8 x). The enriched fragments, which contained a long 3' ssDNA overhang, were incubated with 1 pmol of target specific biotin, surface and loop oligonucleotide (sequence available in suppl. table 1), 40 U Tag DNA Ligase (Enzymatics), 0.25 U Bst DNA Polymerase Full Length (NEB) in ThermoPol® Reaction Buffer (NEB) supplemented with 200 μM dNTP, 1mM NAD⁺ at 50 °C for 30 min. Excess oligonucleotide was then digested with 25 U ExoI for 30 min. at 37 °C, followed by a purification using KAPA Pure beads (1 x). The DNA fragments were digested with BsaI to generate specific overhangs that allow the ligation of surface specific oligonucleotides (PS1420 and PS867) and the second overhang created at the opposite end was used to ligate the loop (PS189 and PS1472). The resulting hairpin molecules were bound on 5 μg of Dynabeads™ MyOne™ Streptavidin T1 (Invitrogen) in PB for 60 min. at room temperature. Beads were washed and resuspended in PB prior to loading into the flow cell.

Determination of FMR1 repeat length and promoter methylation using magnetic tweezers

The prepared hairpin-beads were injected in a flow cell and the small tandem repeat sizes were analysed using our opening assay with ten oligonucleotides capable of forming a three-way junction, which were targeted to hybridize specifically to invariable sequences located downstream and upstream from the CGG-repeat position. These special oligonucleotides capable of forming a three-way junction during the opening phase contain a single stranded region of 8 to 10 bases depending on the sequence as well as a loop structure complementary to the sequence located upstream of the blocking position. Upon binding, these oligonucleotides cause a transient blockage in the opening of the hairpin, allowing the precise mapping of the position of blockages. The number of repeats was then determined by constructing a histogram of blocking positions and aligning the two flanking constant regions to precisely determine the number of repeats on the variable region. For base modification detection, the anti-m⁵C antibody clone ICC/IF (Diagenode) was added to the flow cell at a 1:500 dilution in ABB6 buffer.

Acknowledgements

We would like to thank all the members of the Depixus team and François-Xavier Lyonnet du Moutier for their inputs and fruitful discussions on different aspects of the work presented here as well as Jean Baptiste Boulé for his

Detecting genetic variation and base modifications in DNA and RNA

insight on 8-oxoG. We would like to thank Harold Gouet and Fangyuan Ding for their initial observations of epigenetic detection using antibodies on the MTs. This work was supported by a Eurostars grant entitled “RNA EPIGENETIX: Developing new tools for epigenetic analysis of RNA molecules using the SIMDEQ sequencing platform” (Reference Number: 9830), an ANR grant entitled MuSeq and a Horizon 2020 grant entitled “CONAN II - Complete Nucleic acid ANalysis at genome scale at ultra-high throughput Phase 2” (EIC-SMEInst-2018-2020 grant # 829965). Part of this work was also supported by the European Research Council grant Magreps [267 862].

Author contributions

T.V., G.R., V.C, D.B., and J.F.A were involved in the development and design of the SDI platform and for its initial testing. J.O and R.M. performed the analysis of DNA base modification as well as participated in the determination of precision of the SDI platform. Z.W., and A.L. performed experiments on RNA base modification detection as well as the analysis of RNA using oligonucleotides. J.M., and L.G., performed the *E. coli* and human fragment enrichment. P.d’A., D.S. and S.A.M, participated in the statistical analysis of the results as well as data treatment. T.V, V.C., D.B., J.F.A, C.A, G.S. J.O. and GH participated in the design of the experiments. G.S., C.A., G.H., J.O, J.M and Z.W. wrote the manuscript with inputs from all other authors.

Competing Interests

J.M., Z.W., L.G., A.L., T.V., G.R., P.d’A., D.S., S.A-M., R.M. G.S., C.A., J.O. and G.H. are all either current employees or hold positions in the share capital of the company Depixus SAS.

V.C., D.B. and J.F.A are academic founders and shareholders in Depixus SAS.

Materials and correspondence

All requests for sequence, material or additional information should be addressed to Gordon Hamilton at gh@depixus.com

References

1. Levy, S. E. & Myers, R. M. Advancements in Next-Generation Sequencing. (2016). doi:10.1146/annurev-genom-083115-022413
2. Reuter, J. A., Spacek, D. V & Snyder, M. P. Molecular Cell Review High-Throughput Sequencing Technologies. (2015). doi:10.1016/j.molcel.2015.05.004
3. Jaszczyszyn, Y., Thermes, C. & Dijk, E. L. Van. Ten years of next-generation sequencing

- technology. **30**, (2014).
4. Chen, L. *et al.* High Resolution Methylation PCR for Fragile X Analysis: Evidence for Novel FMR1 Methylation Patterns Undetected in Southern Blot Analyses. *NIH Public Access* **13**, 528–538 (2014).
 5. Emerman, A. B. *et al.* NEBNext Direct: A Novel, Rapid, Hybridization-Based Approach for the Capture and Library Conversion of Genomic Regions of Interest. in *Current Protocols in Molecular Biology* **119**, 7.30.1-7.30.24 (John Wiley & Sons, Inc., 2017).
 6. Samorodnitsky, E. *et al.* Evaluation of Hybridization Capture Versus Amplicon-Based Methods for Whole-Exome Sequencing. *Hum. Mutat.* **36**, 903–914 (2015).
 7. Gnirke, A. *et al.* Solution hybrid selection with ultra-long oligonucleotides for massively parallel targeted sequencing. *Nat. Biotechnol.* **27**, 182–9 (2009).
 8. Kozarewa, I., Armisen, J., Gardner, A. F., Slatko, B. E. & Hendrickson, C. L. Overview of Target Enrichment Strategies. in *Current Protocols in Molecular Biology* **112**, 7.21.1-7.21.23 (John Wiley & Sons, Inc., 2015).
 9. Van Dijk, E. L., Jaszczyszyn, Y. & Thermes, C. Library preparation methods for next-generation sequencing: Tone down the bias. *Exp. Cell Res.* **322**, 12–20 (2014).
 10. Gabrieli, T., Sharim, H., Michaeli, Y. & Ebenstein, Y. Cas9-Assisted Targeting of CHromosome segments (CATCH) for targeted nanopore sequencing and optical genome mapping. *bioRxiv* 1–11 (2017). doi:10.1101/110163
 11. Hafford-Tear, N. J. *et al.* CRISPR/Cas9-targeted enrichment and long-read sequencing of the Fuchs endothelial corneal dystrophy-associated TCF4 triplet repeat. *Genet. Med.* (2019). doi:10.1038/s41436-019-0453-x
 12. Stevens, R. C. *et al.* A novel CRISPR/Cas9 associated technology for sequence-specific nucleic acid enrichment. *PLoS One* **14**, e0215441 (2019).
 13. Slesarev, A. *et al.* CRISPR/Cas9 targeted CAPTURE of mammalian genomic regions for characterization by NGS. *Sci. Rep.* **9**, (2019).
 14. Treutlein, B., Gokce, O., Quake, S. R. & Südhof, T. C. Cartography of neurexin alternative splicing mapped by single-molecule long-read mRNA sequencing. *Proc. Natl. Acad. Sci. U. S. A.* **111**, E1291-9 (2014).
 15. Vollmers, C., Penland, L., Kanbar, J. N. & Quake, S. R. Novel exons and splice variants in the human antibody heavy chain identified by single cell and single molecule sequencing. *PLoS One* **10**, 1–9 (2015).

Detecting genetic variation and base modifications in DNA and RNA

16. Fiorini, F., Bagchi, D., Le Hir, H. & Croquette, V. Human Upf1 is a highly processive RNA helicase and translocase with RNP remodelling activities. *Nat. Commun.* **6**, 7581 (2015).
17. Manosas, M. *et al.* Mechanism of strand displacement synthesis by DNA replicative polymerases. *Nucleic Acids Res.* **40**, 6174–6186 (2012).
18. Maier, B., Bensimon, D. & Croquette, V. Replication by a single DNA polymerase of a stretched single-stranded DNA. *Proc. Natl. Acad. Sci. U. S. A.* **97**, 12002–7 (2000).
19. Manosas, M., Spiering, M. M., Ding, F., Croquette, V. & Benkovic, S. J. Collaborative coupling between polymerase and helicase for leading-strand synthesis. *Nucleic Acids Res.* **40**, 6187–6198 (2012).
20. Manosas, M. *et al.* Magnetic Tweezers for the Study of DNA Tracking Motors. in *Methods in enzymology* **475**, 297–320 (2010).
21. Gosse, C. & Croquette, V. Magnetic Tweezers: Micromanipulation and Force Measurement at the Molecular Level. *Biophys. J.* **82**, 3314–3329 (2002).
22. Ding, F. *et al.* Single-molecule mechanical identification and sequencing. *Nat. Methods* **9**, 367–72 (2012).
23. Bland, C. S. *et al.* Global regulation of alternative splicing during myogenic differentiation. *Nucleic Acids Res.* **38**, 7651–7664 (2010).
24. PacBio, N. & PacBio, N. Detecting DNA Base Modifications Using Single Molecule, Real-Time Sequencing. *Genome Announc.* **2**, 1–5 (2015).
25. Kriegel, F., Ermann, N. & Lipfert, J. Probing the mechanical properties, conformational changes, and interactions of nucleic acids with magnetic tweezers. *J. Struct. Biol.* **197**, 26–36 (2017).
26. Zhang, C. *et al.* The Mechanical Properties of RNA-DNA Hybrid Duplex Stretched by Magnetic Tweezers. *Biophys. J.* **116**, 196–204 (2019).
27. Melkonyan, L., Bercy, M., Bizebard, T. & Bockelmann, U. Overstretching Double-Stranded RNA, Double-Stranded DNA, and RNA-DNA Duplexes. *Biophys. J.* **117**, 509–519 (2019).
28. Kahramanoglou, C. *et al.* Genomics of DNA cytosine methylation in *Escherichia coli* reveals its role in stationary phase transcription. *Nat. Commun.* **3**, (2012).
29. Wasserkort, R. *et al.* Aberrant septin 9 DNA methylation in colorectal cancer is restricted to a single CpG island. *BMC Cancer* **13**, 398 (2013).
30. Lind, G. E. *et al.* Identification of an epigenetic biomarker panel with high sensitivity and

- specificity for colorectal cancer and adenomas. *Mol. Cancer* **10**, 85 (2011).
31. Lam, K., Pan, K., Linnekamp, J. F., Medema, J. P. & Kandimalla, R. DNA methylation based biomarkers in colorectal cancer: A systematic review. *Biochim. Biophys. Acta - Rev. Cancer* **1866**, 106–120 (2016).
 32. Santoro, M. R., Bray, S. M. & Warren, S. T. Molecular Mechanisms of Fragile X Syndrome: A Twenty-Year Perspective. *Annu. Rev. Pathol. Mech. Dis.* **7**, 219–245 (2012).
 33. Mor-Shaked, H. & Eiges, R. Reevaluation of FMR1 hypermethylation timing in fragile X syndrome. *Front. Mol. Neurosci.* **11**, 1–7 (2018).
 34. Chen, L. *et al.* High-resolution methylation polymerase chain reaction for fragile X analysis: Evidence for novel FMR1 methylation patterns undetected in Southern blot analyses. *Genet. Med.* **13**, 528–538 (2011).
 35. Schwartz, S. & Motorin, Y. RNA Biology Next-generation sequencing technologies for detection of modified nucleotides in RNAs Next-generation sequencing technologies for detection of modified nucleotides in RNAs. (2016). doi:10.1080/15476286.2016.1251543
 36. Chakravorty, S. & Hegde, M. Gene and Variant Annotation for Mendelian Disorders in the Era of Advanced Sequencing Technologies. (2017). doi:10.1146/annurev-genom-083115
 37. Schwartzman, O. & Tanay, A. Single-cell omics Single-cell epigenomics: techniques and emerging applications. *Nat. Publ. Gr.* (2015). doi:10.1038/nrg3980
 38. Sueoka, T., Koyama, K., Hayashi, G. & Okamoto, A. Chemistry-Driven Epigenetic Investigation of Histone and DNA Modifications. *Chem. Rec.* **18**, 1727–1744 (2018).
 39. Clark, T. A., Spittle, K. E., Turner, S. W. & Korlach, J. *Direct Detection and Sequencing of Damaged DNA Bases. Genome Integrity* **2**, (2011).
 40. Davis, B. M., Chao, M. C. & Waldor, M. K. Entering the era of bacterial epigenomics with single molecule real time DNA sequencing. doi:10.1016/j.mib.2013.01.011
 41. Liu, L. *et al.* Recent Advances in the Genomic Profiling of Bacterial Epigenetic Modifications. *Biotechnol. J.* **14**, 1–6 (2019).
 42. Liu, Q., Georgieva, D. C., Egli, D. & Wang, K. NanoMod: a computational tool to detect DNA modifications using Nanopore long-read sequencing data. doi:10.1186/s12864-018-5372-8
 43. Liu, Q. *et al.* Detection of DNA base modifications by deep recurrent neural network on Oxford Nanopore sequencing data. doi:10.1038/s41467-019-10168-2

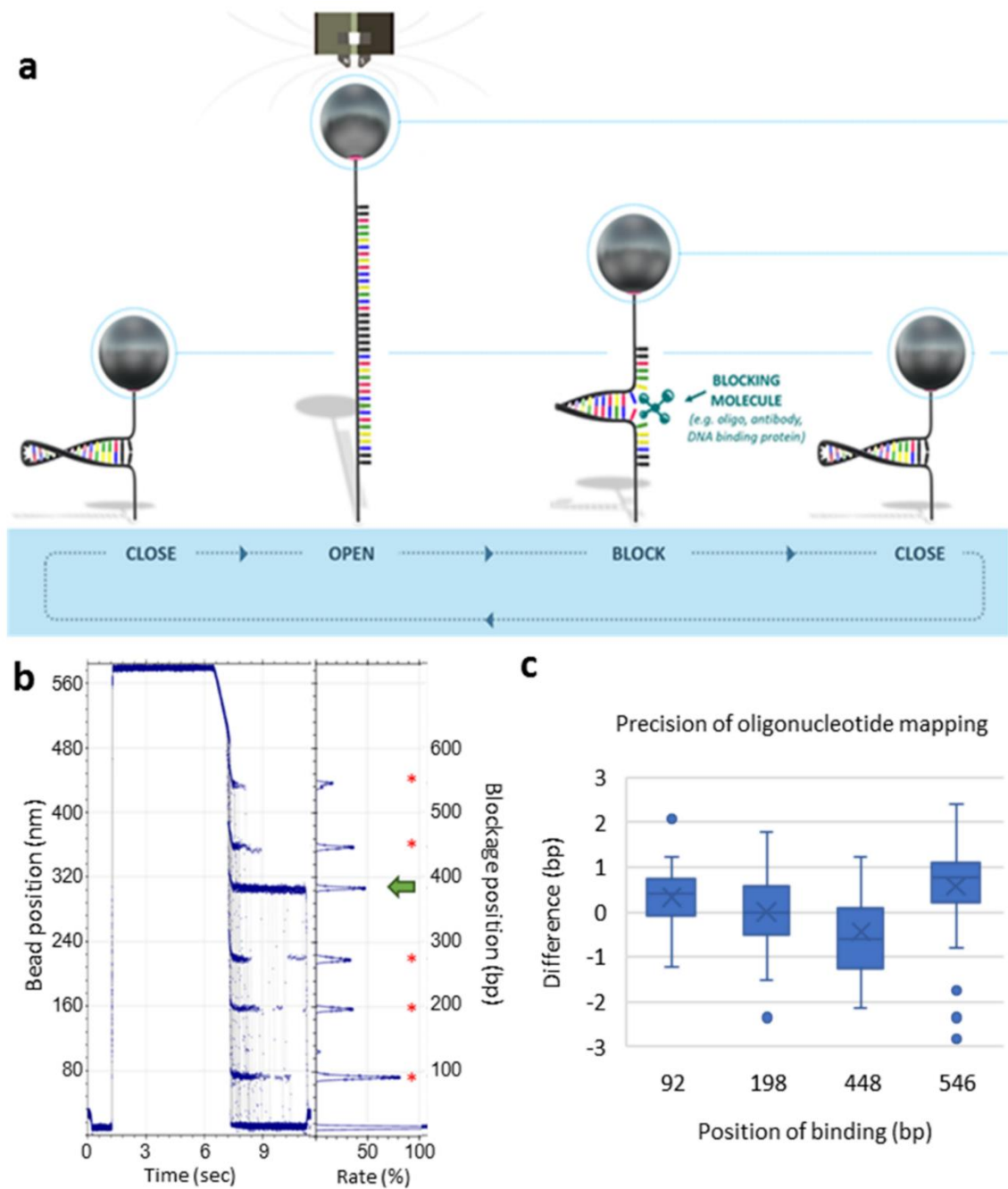
Detecting genetic variation and base modifications in DNA and RNA

44. Flusberg, B. A. *et al.* Direct detection of DNA methylation during single-molecule, real-time sequencing. *Nat. Publ. Gr.* (2010). doi:10.1038/nmeth.1459
 45. Laird, P. W. Restriction-modification system Principles and challenges of genome-wide DNA methylation analysis. *Nat. Rev. Genet.* (2010). doi:10.1038/nrg2732
 46. Meaburn, E. & Schulz, R. Next generation sequencing in epigenetics: Insights and challenges. *Semin. Cell Dev. Biol.* **23**, 192–199 (2012).
 47. Grozhik, A. V & Jaffrey, S. R. Distinguishing RNA modifications from noise in epitranscriptome maps. *Nat. Chem. Biol.* **14**, 215–225 (2018).
 48. Peluso, P. *et al.* Sequencing the unsequenceable: Expanded CGG-repeat alleles of the fragile X gene. *Genome Res.* **23**, 121–128 (2012).
 49. Giesselmann, P. *et al.* Analysis of short tandem repeat expansions and their methylation state with nanopore sequencing. *Nat. Biotechnol.* *2019* 1–4 (2019). doi:10.1038/s41587-019-0293-x
 50. Graves, E. T. *et al.* A dynamic DNA-repair complex observed by correlative single-molecule nanomanipulation and fluorescence. **4**, (2015).
-

Detecting genetic variation and base modifications in DNA and RNA

Figures and tables

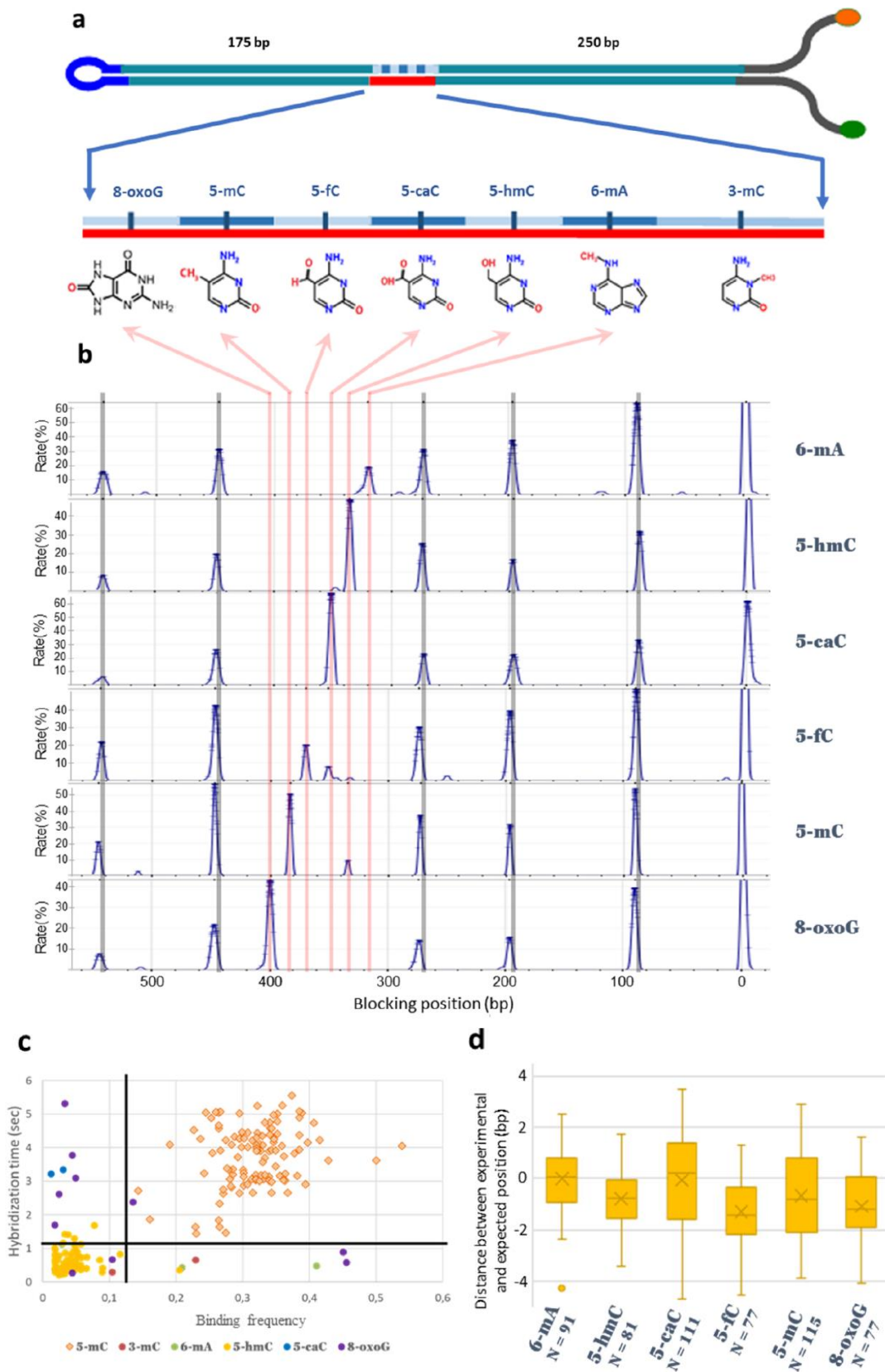
Figure 1. Principle and resolution of the new SDI platform.



(a) Schematic representation of a typical MT cycle. When the force increases, by approaching the magnets to the sample, the DNA hairpin molecule is denatured and binding molecules (either oligonucleotides or proteins) bind to the ssDNA nucleic acid. Upon reduction in force, the hairpin reforms and transient blockages occur at the binding positions. **(b)** All the cycles are overlaid, and a cumulative histogram of the blocking positions is built. In this example, a 10-base reference oligonucleotide that binds five times (red asterisks) was injected at the same time as an antibody against m^5C modification (green arrow). **(c)** Mapping of reference blocking positions of a 10 DNA base oligonucleotide on a 600 bp hairpin ($n=80$ individual molecules). The average experimental positions versus the expected positions were between \pm one base for the majority of the molecules. Whisker boxes represent 50% of the points with the average as a line within the box and the median as a cross.

Detecting genetic variation and base modifications in DNA and RNA

Figure 2. Detection and precise mapping of DNA base modifications.



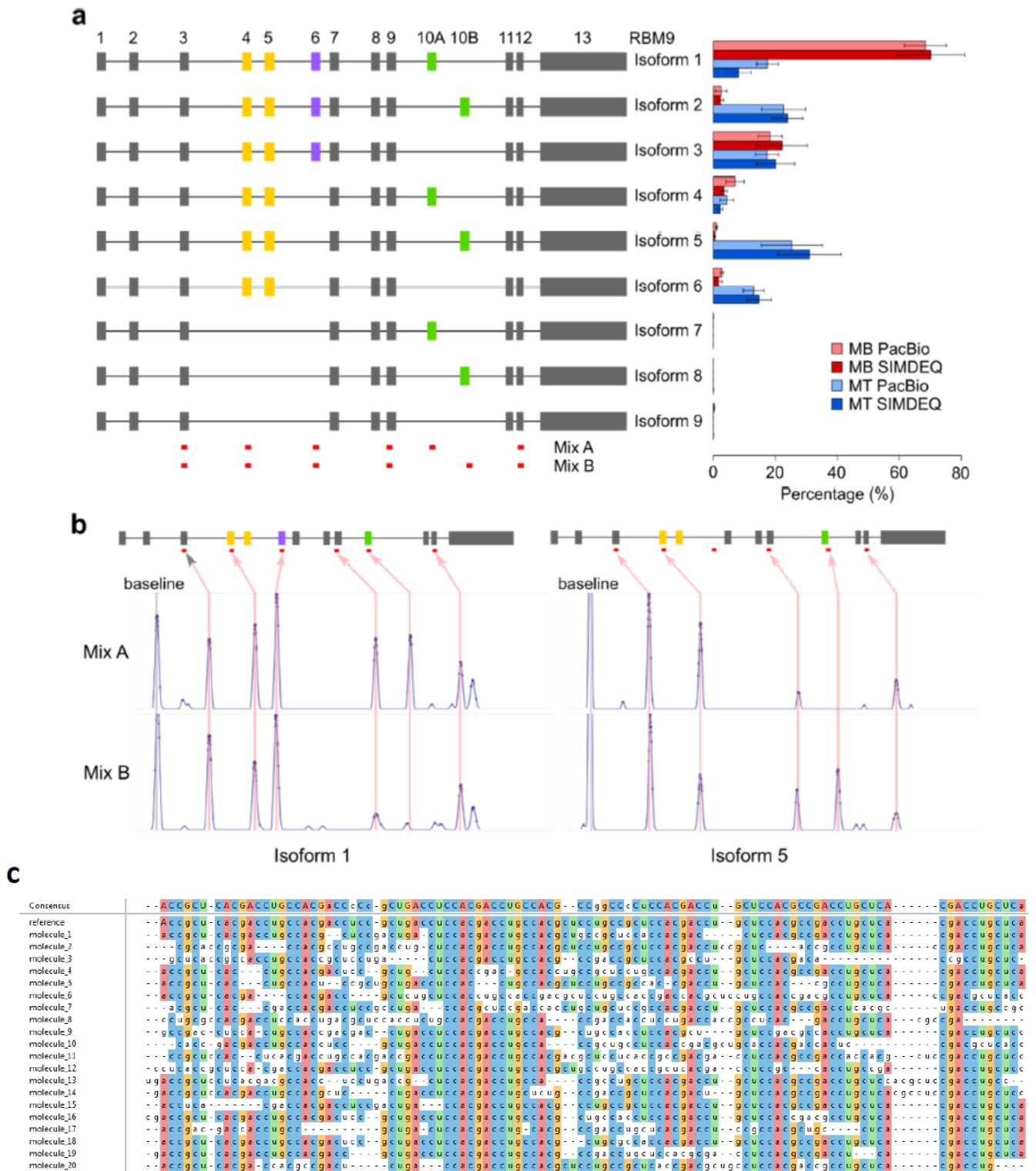
(a) Schematic representation of the hairpin constructed with seven different base modifications. Each oligonucleotide contained a DNA base modification and the linker was constructed by annealing on a splint

Detecting genetic variation and base modifications in DNA and RNA

template. **(b)** Detection of six out of the seven modifications present on the same molecule by sequentially injecting the antibody corresponding to each base modification. The six different experiments were aligned using the reference oligonucleotide bindings. **(c)** By plotting the hybridization time versus binding frequency, it is possible to cluster true positives (in this case, the m⁵C modification with the anti-m⁵C antibody) from the false positives (principally the hm5C modification). Each point represents the cumulative binding data for the m⁵C antibody as determined for each modified base on each individual hairpin (note that for many hairpins, there were no false binding events, so fewer points are plotted). By thresholding the time and frequency, we can eliminate the false positives. **(d)** Antibody binding positions were mapped to the hairpin molecule within 1 bp resolution for the majority of the molecules. Whisker boxes represent 50% of the points with the average as a line within the box and the median as a cross.

Detecting genetic variation and base modifications in DNA and RNA

Figure 3. Identification of alternative splicing isoforms using fingerprinting oligonucleotides.



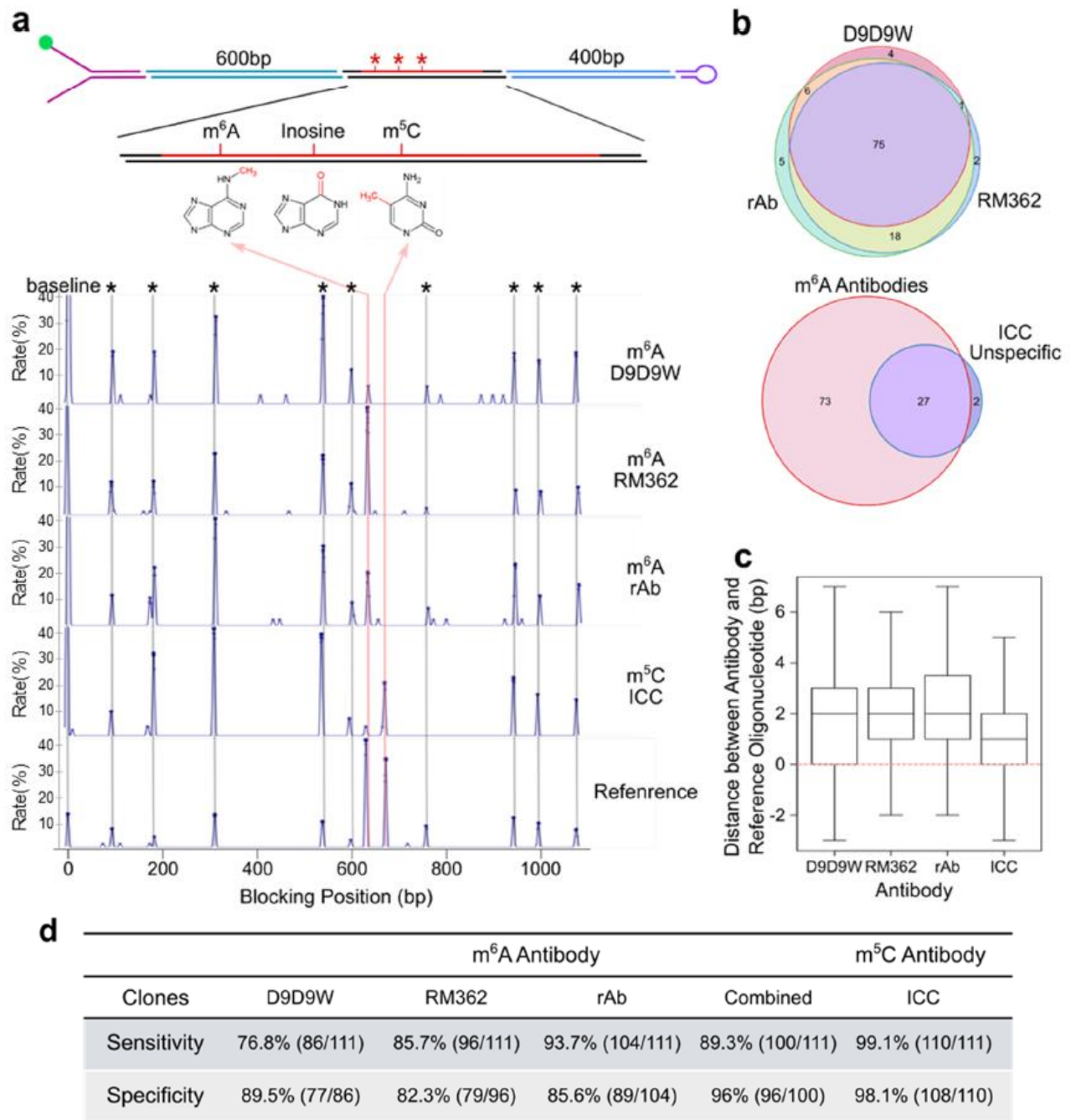
(a) A schematic showing nine different possible isoforms from mouse RBM9 transcripts. RNAs from two different cell types were used (myoblast, MB and myotube, MT), and different isoforms were quantified using the MT platform or PacBio sequencing of long reads. The comparison between different identification methods as well as changes in alternative splicing isoforms are shown on the right. (b) Examples of cDNA from two different isoforms generating specific signatures with the two oligonucleotide mixes to differentiate transcripts with either a 10a or

Detecting genetic variation and base modifications in DNA and RNA

10b exon. (c) The alignment of reconstructed sequence from 20 individual molecules of RNA and the consensus sequence obtained from these sequences. The expected sequence (referred as reference) is indicated. Each base within a column that corresponds to the reference sequenced is coloured. The consensus sequence showed 5 errors compared to the expected reference sequence.

Detecting genetic variation and base modifications in DNA and RNA

Figure 4. Detection of RNA base modifications.



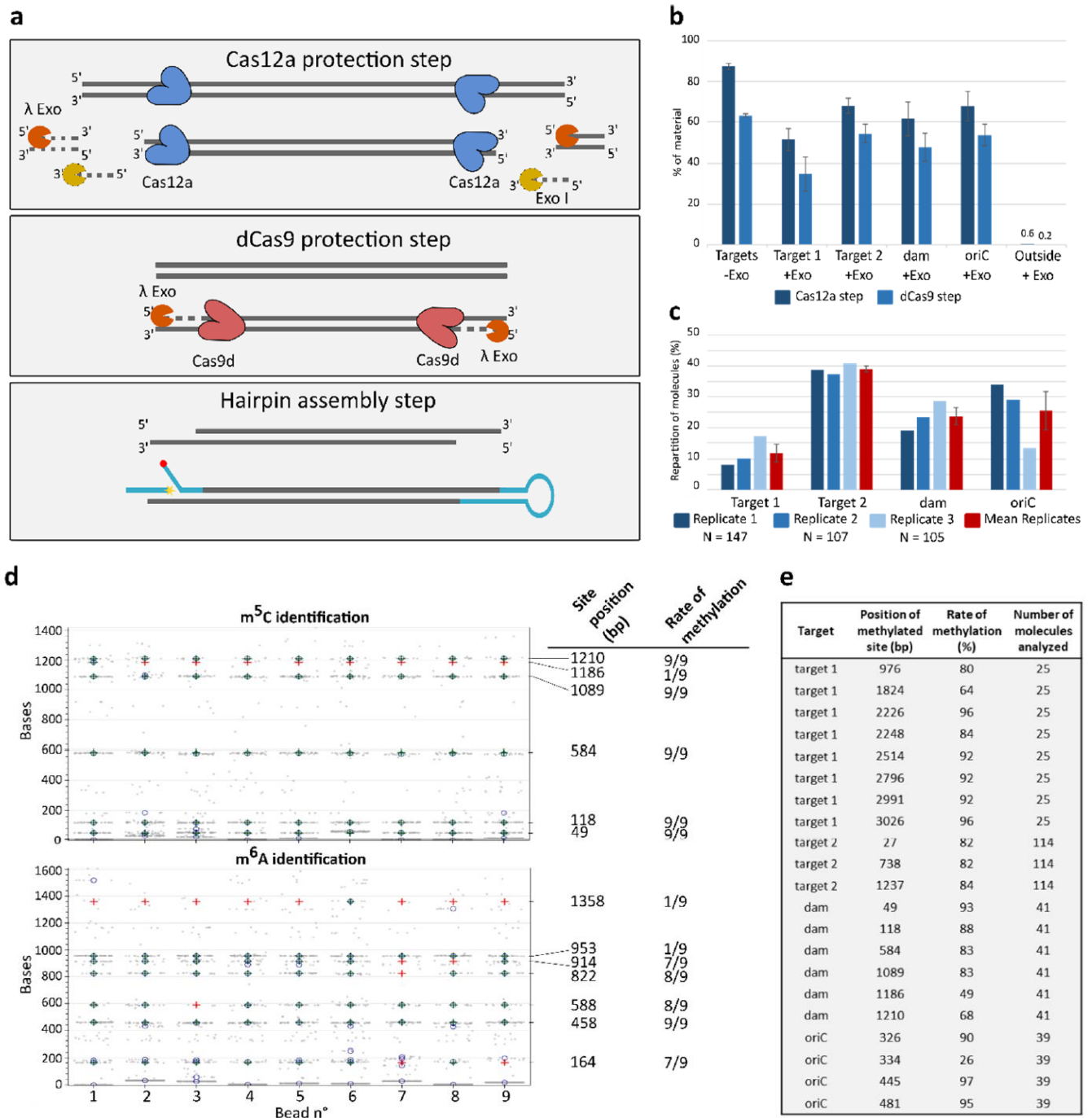
(a) Representation of the synthetic hairpin constructed for epigenetic detection on RNA. The binding position histogram of specific antibodies as well as a reference oligonucleotide mix binding on a single hairpin is shown below. The reference oligonucleotides peaks are marked with an asterisk (*), and are used for alignment. The antibody binding positions are shown by the red line. The last histogram represents the reference oligonucleotide binding positions that correspond to the same position as the modification. **(b)** Venn diagram showing the overlap between three different m⁶A antibody clones (top). Below, the Venn diagram shows the overlap between non-specific binding identified by m⁵C antibody (ICC) at the position of m⁶A modification, and the binding positions identified by at least two out of three m⁶A antibodies. **(c)** Boxplot showing the distance of binding between antibody and the reference oligonucleotides is base pair resolution for all antibodies tested. Whisker boxes represent 50% of

Detecting genetic variation and base modifications in DNA and RNA

the points with the average as a line within the box and the median as a cross. **(d)** Table showing the sensitivity and the specificity of all three m⁶A antibodies and the m⁵C antibody tested. For the combined analysis of m⁶A antibodies, a binding position was considered as such if it is recognized by at least two out of the three antibodies tested.

Detecting genetic variation and base modifications in DNA and RNA

Figure 5. Enrichment of specific genomic regions using a CRISPR-based method.



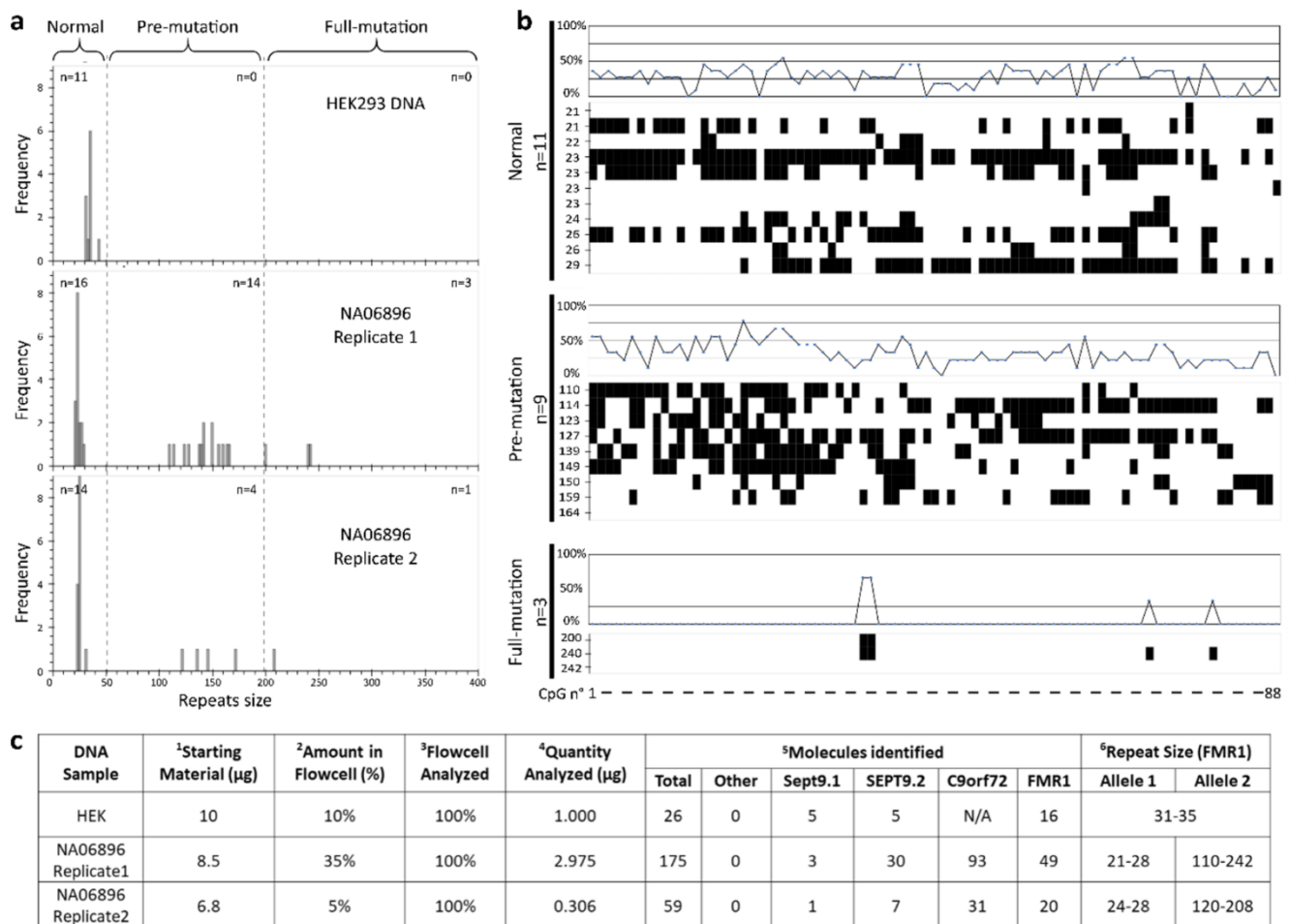
(a) The protocol is divided into two steps: 1) Targeting the region of interest by two Cas12a complexes, followed by digestion with exonucleases. 2) Dead Cas9 protection, followed by lambda exonuclease digestion to generate ssDNA overhangs at each end that are used to assemble the hairpins. (b) qPCR of enrichment of four *E. coli* targets. A control excluding the exonucleases was included (to account for purification lost) and a positive control for digestion was performed by quantifying off-target DNA. Protection was measured for each target after the Cas12a (dark blue) and dCas9 (light blue) steps. Bars represent the average protected material from three biological replicates + s.e.m, $n=3$. (c) Repartition of target molecules analysed on the MT platform from three biological replicates (shades of blue) and their average (red bars). (d) Detection of m⁵C and m⁶A on the same enriched *dam*

Detecting genetic variation and base modifications in DNA and RNA

molecules (each column represents a single molecule, and in each panel, the same column corresponds to the same bead). Grey points indicate detected binding events and the expected modification positions are indicated on the right axis. Blue crosses indicate detected blockages corresponding to the modification and red crosses indicate expected positions where methylation was not detected. **(e)** Analysis of m⁵C methylation of all the isolated *E. coli* fragments for all three biological replicates. The CCwGG site positions within the hairpins are indicated as well as their rate of methylation.

Detecting genetic variation and base modifications in DNA and RNA

Figure 6. Analysis of repeat length and methylation status of the FMR1 locus.



(a) Histograms of the distribution of CGG repeat length for FMR1 on two DNA samples (HEK DNA, and the clinical sample, NA06896). The n represents the number of molecules identified in three categories, normal (<50 repeats), pre-mutation (50 to 200 repeats) and full-mutation (>200 repeats). (b) Cytosine methylation analysis of the CpG island located within the FMR1 promotor region of DNA sample NA06896. All CpG or non-CpG sites are represented on the X axis (the list and position of sites are in Supplemental Table 1). Molecules are ordered by repeat size and grouped by mutation status (normal, pre-mutation, full-mutation). Line graphs represent the frequency of molecules identified as methylated for a specific CpG or non-CpG site within this population. (c) The table summarizing the libraries prepared and the results obtained from these samples. **1.** Amount of DNA used to prepare the library, **2.** Amount of starting material injected in the flow cell, **3.** Proportion of the flow cell analysed, **4.** Relative quantity of starting material analysed, **5.** Number of molecules analysed on the MT platform and repartition according to the oligonucleotide binding pattern, **6.** Quantification of FMR1 repeat size, N/A: Not included in the library preparation.

Detecting genetic variation and base modifications in DNA and RNA

Table 1. Sensitivity and specificity of DNA base detection with MTs using our antibody-based approach.

<i>DNA-base modification</i>	<i>8oxoG</i>	<i>m⁵C</i>	<i>hm⁵C</i>	<i>ca⁵C</i>	<i>m⁶A</i>	<i>f⁵C</i>
<i>Sensitivity of detection</i>	100%	98%	95%	98%	100%	100%
<i>Specificity of detection</i>	100%	100%	98%	100%	100%	100%

Sensitivity is defined as the percentage of molecules in which the modification was successfully detected using the antibody among all the molecules observed, and specificity as the number of molecules where the modification corresponding to the antibody was correctly identified among all the blockages detected on each bead (either through thresholding or cross-reference between different antibodies).